

# Efficient simulation of multidimensional phonon transport using energy-based variance-reduced Monte Carlo formulations

Jean-Philippe M. Péraud and Nicolas G. Hadjiconstantinou  
Department of Mechanical Engineering, Massachusetts Institute of Technology  
Cambridge, MA 02139, USA

September 9, 2018

## Abstract

We present a new Monte Carlo method for obtaining solutions of the Boltzmann equation for describing phonon transport in micro and nanoscale devices. The proposed method can resolve arbitrarily small signals (e.g. temperature differences) at small constant cost and thus represents a considerable improvement compared to traditional Monte Carlo methods whose cost increases quadratically with decreasing signal. This is achieved via a control-variate variance reduction formulation in which the stochastic particle description only solves for the deviation from a nearby equilibrium, while the latter is described analytically. We also show that simulating an energy-based Boltzmann equation results in an algorithm that lends itself naturally to exact energy conservation thereby considerably improving the simulation fidelity. Simulations using the proposed method are used to investigate the effect of porosity on the effective thermal conductivity of silicon. We also present simulations of a recently developed thermal conductivity spectroscopy process. The latter simulations demonstrate how the computational gains introduced by the proposed method enable the simulation of otherwise intractable multiscale phenomena.

## 1 Introduction

Over the past two decades, the dramatic advances associated with MEMS (Micro Electro Mechanical Systems) and NEMS (Nano Electro Mechanical Systems) have attracted considerable attention on microscale and nanoscale heat transfer considerations [1]. Applications range from thermal management of electronic devices [2] to the development of thermoelectric materials with higher figure of merit [3]. The thermoelectric figure of merit is proportional to the electrical conductivity and inversely proportional to thermal conductivity and can thus be improved by reducing the latter and/or increasing the former. One of the most promising approaches towards reducing the thermal conductivity of thermoelectric materials is the introduction of nanostructures that interact

with the ballistic motion of phonons at small scales thus influencing heat transport [4]. Such approach requires a reliable description of phonon transport at the nanoscale and cannot rely on Fourier’s law, which is valid for diffuse transport. On the other hand, first principles calculations (e.g. molecular dynamics approaches, classical or quantum mechanical) are too expensive for treating phonon transport at the device (e.g. micrometer) scale. At these scales, a kinetic description based on the Boltzmann Transport Equation (BTE) offers a reasonable balance between fidelity and model complexity and is able to accurately describe the transition from diffusive to ballistic transport as characteristic system lengthscales approach and ultimately become smaller than the phonon mean free path.

Solving the BTE is a challenging task, especially in complex geometries. The high dimensionality of the distribution function coupled with the ability of particle methods to naturally simulate advection processes without stability problems [5] make particle Monte Carlo methods particularly appealing. Following the development of the Direct Monte Carlo Method by Bird [6] for treating dilute gases, Monte Carlo methods for phonon transport were first introduced by Peterson [7] and subsequently improved by Mazumder and Majumdar [8]. Over the past decade, further important refinements have been introduced: Lacroix *et al.* introduced a method to treat frequency dependent mean free paths [9]; Jeng *et al.* introduced a method for efficiently treating transmission and reflection of phonons at material interfaces and used this method to model the thermal conductivity of nanoparticle composites [4]. Hao *et al.* developed [10] a formulation for periodic boundary conditions in order to study the thermal conductivity of periodic nanoporous materials while only simulating one unit cell (period).

The work presented here introduces a number of improvements which enable efficient and accurate simulation of the most challenging phonon transport problems, namely three-dimensional and transient. Accuracy is improved compared to previous approaches by introducing an energy-based formulation, which simulates energy packets rather than phonons; this formulation makes energy conservation particularly easy to implement rigorously, in contrast to previous approaches which were ad-hoc and in many cases ineffective. We also introduce a variance-reduced formulation for *substantially* reducing the statistical uncertainty associated with sampling solution (temperature and heat flux) fields. This formulation is based on the concept of control variates, first introduced in the context of Monte Carlo solutions of the Boltzmann equation for dilute gases [5]; it is based on the fact that signal strength is intimately linked to deviation from equilibrium, or in other words, that the large computational cost associated with small signals is due to the fact that in these problems the deviation from equilibrium is small. This observation can be exploited by utilizing the nearby equilibrium state as a “control” and using the Monte Carlo method to calculate the contribution of non-equilibrium therefrom. Because the deviation from equilibrium is small, only a small quantity is evaluated stochastically (the fields associated with the equilibrium component are known analytically) resulting in small statistical uncertainty; moreover, the latter decreases as the deviation from equilibrium decreases, thus enabling the simula-

tion of arbitrarily small deviations from equilibrium.

In the technique presented here, we use particles to simulate the deviation from equilibrium, which is thus referred to as a deviational method; the origin of this methodology can be found in the Low Variance Deviational Simulation Monte Carlo (LVDSMC) method [11, 12, 13, 14] recently developed for dilute gases. The theoretical basis underlying this method as well as the modifications required for use in phonon transport simulations are described in section 2.3. The resulting algorithm is described in section 3 and validated in section 4.

The proposed algorithm is used to obtain solutions to two problems of practical interest. The first application studies the thermal conductivity of porous silicon containing voids with different degrees of alignment and is intended to showcase how ballistic effects influence the “effective” thermal conductivity. The second application is related to the recently developed experimental method of “thermal conductivity spectroscopy” [15] based on the pump-probe technique known as transient thermorefectance, which uses the response of a material to laser irradiation to infer information about physical properties of interest [16] (e.g. mean free paths of the dominant heat carriers).

## 2 Theoretical basis

### 2.1 Summary of traditional Monte Carlo simulation methods

We consider the Boltzmann Transport Equation in the frequency-dependent relaxation-time approximation

$$\frac{\partial f}{\partial t} + \mathbf{V}_g(\omega, p) \nabla f = -\frac{f - f^{loc}}{\tau(\omega, p, T)} \quad (1)$$

where,  $f = f(t, \mathbf{r}, \mathbf{k}, p)$  is the phonon distribution in the phase space,  $\omega = \omega(\mathbf{k}, p)$  the phonon radial frequency,  $p$  the phonon polarization and  $T$  the temperature; similarly to the nomenclature adopted in [1],  $f$  is defined in reference to the occupation number. For example, if the system is perfectly thermalized at temperature  $T_{eq}$ ,  $f$  is a Bose-Einstein distribution

$$f_T^{eq} = \frac{1}{\exp\left(\frac{\hbar\omega(\mathbf{k}, p)}{k_b T}\right) - 1} \quad (2)$$

where  $k_b$  is Boltzmann’s constant. Also,  $f^{loc}$  is an equilibrium (Bose-Einstein) distribution corresponding to the *local pseudo-temperature* defined more precisely in section 2.1.2.

In this work we consider Longitudinal Acoustic (LA), Transverse Acoustic (TA), Longitudinal Optical (LO), Transverse Optical (TO) polarizations; acoustic phonons are known to be the most important contributors to lattice thermal conductivity [17, 18]. The phonon radial frequency is given by the dispersion relation  $\omega = \omega(\mathbf{k}, p)$ . Phonons travel at the group velocity  $\mathbf{V}_g = \nabla_{\mathbf{k}} \omega$ .

In the following, we always consider the ideal case where the dispersion relation is isotropic. For convenience, the radial frequency  $\omega$  and two polar angles  $\theta$  and  $\phi$

are usually preferred as primary parameters compared to the wave vector. Equation (1) is simulated using computational particles that represent phonon bundles, namely collections of phonons with similar characteristics (position vector  $\mathbf{x}$ , the wave vector  $\mathbf{k}$ , and the polarization/propagation-mode  $p$ ), using the approximation

$$\frac{1}{8\pi^3}f(t, \mathbf{x}, \mathbf{k}, p) \approx N_{eff} \sum_i \delta^3(\mathbf{x} - \mathbf{x}_i) \delta^3(\mathbf{k} - \mathbf{k}_i) \delta_{p,p_i} \quad (3)$$

where  $\mathbf{x}_i$ ,  $\mathbf{k}_i$  and  $p_i$  respectively represent the position, the wave vector and the polarization of particle  $i$  and  $N_{eff}$  is the number of phonons in each phonon bundle. The factor  $1/8\pi^3$  is necessary for converting the quantity representing the occupation number,  $f$ , into a quantity representing the phonon density in phase space. Written in polar coordinates, and using the frequency instead of the wave number, this expression becomes

$$\frac{D(\omega, p)}{4\pi} f(t, \mathbf{x}, \omega, \theta, \phi, p) \sin(\theta) \approx N_{eff} \sum_i \delta^3(\mathbf{x} - \mathbf{x}_i) \delta(\omega - \omega_i) \delta(\theta - \theta_i) \delta(\phi - \phi_i) \delta_{p,p_i} \quad (4)$$

where  $\omega_i$ ,  $\theta_i$ , and  $\phi_i$  respectively represent the radial frequency, the polar angle and the azimuthal angle of particle  $i$ . The density of states,  $D(\omega, p)$ , is made necessary by the use of  $\omega$  as a primary parameter and is given by

$$D(\omega, p) = \frac{k(\omega, p)^2}{2\pi^2 V_g(\omega, p)} \quad (5)$$

### 2.1.1 Initialization

Systems are typically initialized in an equilibrium state at temperature  $T$ ; the number of phonons in a given volume  $V$  is calculated using the Bose-Einstein statistics

$$N = V \int_{\omega=0}^{\omega_{max}} \sum_p D(\omega, p) f_T^{eq}(\omega) d\omega \quad (6)$$

where:

- $\omega_{max}$  is the maximum (cut-off) frequency
- $f_T^{eq}$  is the occupation number at equilibrium at temperature  $T$

The number of computational particles (each representing a phonon bundle) is given by  $N/N_{eff}$ . The value of  $N_{eff}$  is determined by balancing computational cost (including storage) with the need for a sufficiently large number of particles for statistically meaningful results.

### 2.1.2 Time integration

Once the system is initialized, the simulation proceeds by applying a splitting algorithm with timestep  $\Delta t$ . Integration for one timestep comprises of three substeps:

- The advection substep during which bundle  $i$  moves by  $\mathbf{V}_{g,i}\Delta t$ .
- The sampling substep during which the temperature ( $T$ ) and pseudo-temperature ( $T_{loc}$ ) are locally measured. They are calculated by inverting the local energy ( $E$ ) and pseudo-energy ( $\tilde{E}$ ) [10] relations

$$E = N_{eff} \sum_i \hbar\omega_i = V \int_{\omega=0}^{\omega_{max}} \sum_p \frac{D(\omega, p)\hbar\omega}{\exp\left(\frac{\hbar\omega}{k_b T}\right) - 1} d\omega \quad (7)$$

and

$$\tilde{E} = N_{eff} \sum_i \frac{\hbar\omega_i}{\tau(\omega_i, p_i, T)} = V \int_{\omega=0}^{\omega_{max}} \sum_p \frac{D(\omega, p)\hbar\omega}{\tau(\omega, p, T)} \frac{1}{\exp\left(\frac{\hbar\omega}{k_b T_{loc}}\right) - 1} d\omega \quad (8)$$

respectively.

- The scattering substep, during which each phonon  $i$  is scattered according to its scattering probability given by

$$P_i = 1 - \exp\left(-\frac{\Delta t}{\tau(\omega_i, p_i, T)}\right) \quad (9)$$

Scattering proceeds by drawing new frequencies, polarizations and traveling directions. Because of the frequency dependent relaxation times, frequencies must be drawn from the distribution  $D(\omega, p)f^{loc}/\tau(\omega, p, T)$ . Since scattering events conserve energy, the latter must be conserved during this substep. However, because the frequencies of the scattered phonons are drawn randomly, conservation of energy is enforced by adding or deleting particles until a target energy is approximately reached [8, 9]. In addition to being approximate, this method does not always ensure that energy is conserved, resulting in random walks in the energy of the simulated system, which in some cases leads to deterministic error. In the next section, we present a convenient way for rigorously conserving energy.

## 2.2 Energy based formulation

While most computational techniques developed so far only conserve energy in an approximate manner [8, 9], here we show that an energy-based formulation provides a convenient and rigorous way to conserve energy in the relaxation time approximation.

Adopting a similar approach as in [2] to derive the *Equation of Phonon Radiative Transfer*, we multiply (1) by  $\hbar\omega$  to obtain

$$\frac{\partial e}{\partial t} + \mathbf{V}_g \nabla e = \frac{e^{loc} - e}{\tau} \quad (10)$$

which we will refer to as the energy-based BTE. Here,  $e = \hbar\omega f$  and  $e^{loc} = \hbar\omega f^{loc}$ . Equation (10) can be simulated by writing

$$e \approx 8\pi^3 \mathcal{E}_{eff} \sum_i \delta^3(\mathbf{x} - \mathbf{x}_i) \delta^3(\mathbf{k} - \mathbf{k}_i) \delta_{p,p_i} \quad (11)$$

where  $\mathcal{E}_{eff}$  is defined as the effective energy carried by each computational particle. Statement (11) defines computational particles that all represent the same amount of energy. From the point of view of phonons, comparing (3) and (11) shows that the effective number of phonons represented by the newly defined particles is variable and is linked to the effective energy by the relation  $\mathcal{E}_{eff} = N_{eff} \hbar\omega$ . By analogy with the description of section 2.1, computational particles defined by (11) obey the same computational rules as in the previous Monte Carlo approaches. Modifications appear at three levels:

- When drawing particle frequencies during initialization, emission from boundaries or scattering, the distribution functions that we use must account for the factor  $\hbar\omega$ . For example, when initializing an equilibrium population of particles at a temperature  $T$ , one has to draw the frequencies from the distribution

$$\frac{\hbar\omega \sum_p D(\omega, p)}{\exp\left(\frac{\hbar\omega}{k_b T}\right) - 1} \quad (12)$$

- Calculating the energy in a cell is straightforward and simply consists in counting the number of computational particles. The energy associated with  $N$  particles is given by  $\mathcal{E}_{eff} N$ .
- Since the energy in a cell is proportional to the number of particles, there is no need for an addition/deletion process: *energy is strictly and automatically conserved by simply conserving the number of particles.*

### 2.3 Deviational formulation

In this section we introduce an additional modification which dramatically decreases the statistical uncertainty associated with Monte Carlo simulations of (10). Our approach belongs to a more general class of control-variate variance reduction methods for solving kinetic equations [5, 11, 19] in which the moments  $\langle R \rangle$  of a given distribution  $f$  are computed by writing

$$\int R f d\mathbf{x} d\mathbf{c} = \int R(f - f^{eq}) d\mathbf{x} d\mathbf{c} + \int R f^{eq} d\mathbf{x} d\mathbf{c} \quad (13)$$

where the first term of the right hand side is computed stochastically and the second term is computed deterministically. If  $f^{eq} \approx f$ , the variance reduction is large because only a small term is determined stochastically (see Figures 1 and 2).

In the present context, this methodology provides significant computational savings when an equilibrium (constant temperature) state exists nearby, which is precisely the regime in which statistical noise becomes problematic (low signals). The degree of variance reduction achieved by this method is quantified in section 5.

Let

$$e_{T_{eq}}^{eq}(\omega) = \frac{\hbar\omega}{\exp\left(\frac{\hbar\omega}{k_b T_{eq}}\right) - 1} \quad (14)$$

where  $T_{eq} \neq T_{eq}(\mathbf{x}, t)$ . Then, it is straightforward to show that  $e^d = e - e_{T_{eq}}^{eq}$  is governed by

$$\frac{\partial e^d}{\partial t} + \mathbf{V}_g \nabla e^d = \frac{(e^{loc} - e_{T_{eq}}^{eq}) - e^d}{\tau} \quad (15)$$

Therefore, by analogy to the standard particle methods for solving the Boltzmann equation, we define computational particles by:

$$e^d = e - e_{T_{eq}}^{eq} \approx 8\pi^3 \mathcal{E}_{eff}^d \sum_i s(i) \delta^3(\mathbf{x} - \mathbf{x}_i) \delta^3(\mathbf{k} - \mathbf{k}_i) \delta_{p,p_i}, \quad s(i) = \pm 1 \quad (16)$$

We will refer to these newly defined computational particles as deviational particles. Clearly, deviational particles may be negative since  $e - e_{T_{eq}}^{eq}$  can be a negative quantity. This is accounted for in the sign term in equation (16). In what follows, we derive evolution rules for deviational particles based on (15).

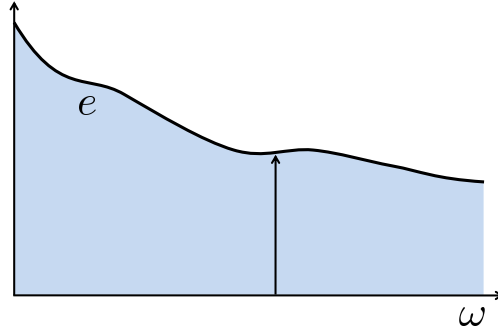


Figure 1: In standard particle methods, the moments of the distribution are stochastically integrated.

### 3 Algorithm

The variance-reduced algorithm is very similar to its non-variance reduced counterpart and comprises an initialization step followed by a splitting algorithm for time integration. The main change lays in the distributions from which deviational particles are sampled.

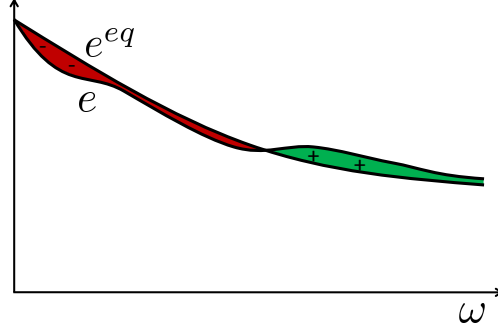


Figure 2: In a control-variate formulation, the stochastic part is reduced to the calculation of the deviation from a known state, which is much smaller.

### 3.1 Initialization

The algorithm proceeds by choosing the equilibrium state at temperature  $T_{eq}$  from which deviations will be simulated. Although this choice can be quite critical in the efficiency of the method (the smaller the deviation from the chosen equilibrium state, the smaller the number of deviational particles required for a given statistical uncertainty, or for a fixed number of deviational particles, the larger the variance reduction), it is usually a natural and intuitive choice.

In some cases, the equilibrium state is the same as the initial state. In such a situation, the simulation starts with no particles. Nevertheless, one still has to choose the deviational effective energy  $\mathcal{E}_{eff}^d$  for subsequent use. In the various examples discussed below, this parameter was chosen as follows: based on a guess of the upper bound on the deviation of temperature at steady state, the deviational energy of the system can be estimated using

$$\Delta E = \int_{\omega=0}^{\omega_{max}} \sum_p \hbar\omega D(\omega, p) \left| \frac{1}{\exp\left(\frac{\hbar\omega}{k_b T}\right) - 1} - \frac{1}{\exp\left(\frac{\hbar\omega}{k_b T_{eq}}\right) - 1} \right| d\omega \quad (17)$$

This estimate of the deviational energy allows  $\mathcal{E}_{eff}^d$  to be (approximately) determined based on the desired number of computational particles.

If the initial state  $f^0$  is different from the equilibrium distribution, particles need to be initialized in the computational domain. Their frequencies and polarizations are drawn from the distribution

$$D(\omega, p)e^d(\omega) = \hbar\omega D(\omega, p) \left[ f^0 - \frac{1}{\exp\left(\frac{\hbar\omega}{k_b T_{eq}}\right) - 1} \right] \quad (18)$$

Typically,  $f^0$  is an equilibrium distribution at some temperature  $T$ , whereby the above



expression reduces to

$$D(\omega, p)e^d(\omega) = \hbar\omega D(\omega, p) \left[ \frac{1}{\exp\left(\frac{\hbar\omega}{k_b T}\right) - 1} - \frac{1}{\exp\left(\frac{\hbar\omega}{k_b T_{eq}}\right) - 1} \right] \quad (19)$$

This function is positive if  $T > T_{eq}$  and negative if  $T < T_{eq}$ . As a result, in the latter case, particles are assigned a negative sign. Drawing the frequencies is performed as in [8], namely by subdividing the frequency range in bins (generally, about 1000 bins are considered enough), defining a discretized and normalized cumulative distribution from (19), uniformly drawing a random number between 0 and 1 and finding the bins it corresponds to in order to match the normalized cumulative distribution.

### 3.2 Advection

Since the left hand side of (15) is analogous to that of (1), the advection substep is unchanged. In other words, during the time step  $\Delta t$ , particles of group velocity  $\mathbf{V}_g(\omega, p)$  are simply advected by  $\mathbf{V}_g(\omega, p)\Delta t$ .

### 3.3 Sampling substep

Sampling the local temperature and pseudo-temperature requires a few changes from the non-variance reduced method, namely

- Let  $C_j$  be the set of indexes corresponding to the particles inside cell  $j$  of volume  $V_j$  at time  $t$ . Since each particle represents the same amount of energy, the deviational energy is given by

$$\Delta E_j = \mathcal{E}_{eff}^d \sum_{i \in C_j} s(i) = \mathcal{E}_{eff}^d (\mathcal{N}_j^+ - \mathcal{N}_j^-) \quad (20)$$

where  $\mathcal{N}_j^+$  and  $\mathcal{N}_j^-$  are respectively the number of positive and negative particles inside the cell  $j$ .

- The corresponding temperature  $T_j$  is then calculated by numerically inverting the expression

$$\frac{\Delta E_j}{V_j} = \int_{\omega=0}^{\omega_{max}} \sum_p D(\omega, p) \hbar\omega \left[ \frac{1}{\exp\left(\frac{\hbar\omega}{k_b T_j}\right) - 1} - \frac{1}{\exp\left(\frac{\hbar\omega}{k_b T_{eq}}\right) - 1} \right] d\omega \quad (21)$$

- Similarly, once  $T_j$  is known, the deviational pseudo-energy is computed using

$$\Delta \tilde{E}_j = \mathcal{E}_{eff}^d \sum_{i \in C_j} \frac{s(i)}{\tau(\omega_i, p_i, T_j)} \quad (22)$$

- The corresponding pseudo-temperature  $[T_{loc}]_j$  is calculated by numerically inverting

$$\frac{\Delta \tilde{E}_j}{V_j} = \int_{\omega=0}^{\omega_{max}} \sum_p \frac{D(\omega, p) \hbar \omega}{\tau(\omega, p, T_j)} \left[ \frac{1}{\exp\left(\frac{\hbar \omega}{k_b [T_{loc}]_j} - 1\right)} - \frac{1}{\exp\left(\frac{\hbar \omega}{k_b T_{eq}} - 1\right)} \right] d\omega \quad (23)$$

### 3.4 Scattering step

During the scattering step we integrate

$$\frac{de^d}{dt} = \frac{(e^{loc} - e_{T_{eq}}^{eq}) - e^d}{\tau(\omega, p, T_j)} \quad (24)$$

for a timestep  $\Delta t$ , where

$$e^{loc} - e_{T_{eq}}^{eq} = \hbar \omega \left[ \frac{1}{\exp\left(\frac{\hbar \omega}{k_b [T_{loc}]_j} - 1\right)} - \frac{1}{\exp\left(\frac{\hbar \omega}{k_b T_{eq}} - 1\right)} \right] \quad (25)$$

We select the particles to be scattered according to the scattering probability (specific to each particle's frequency and polarization, and depending on the local temperature)

$$P(\omega_i, p_i, T_j) = 1 - \exp\left(-\frac{\Delta t}{\tau(\omega_i, p_i, T_j)}\right) \quad (26)$$

The pool of selected particles represent a certain amount of deviational energy  $\mathcal{E}_{eff}^d(\mathcal{N}_{s,j}^+ - \mathcal{N}_{s,j}^-)$ , where  $\mathcal{N}_{s,j}^+$  and  $\mathcal{N}_{s,j}^-$  refer respectively to the number of positive and negative selected (i.e. scattered) particles in cell  $j$ . This pool of selected particles must be replaced by particles with properties drawn from the distribution

$$\frac{D(\omega, p)(e^{loc} - e_{T_{eq}}^{eq})}{\tau(\omega, p, T_j)} = \frac{D(\omega, p) \hbar \omega}{\tau(\omega, p, T_j)} \left( \frac{1}{\exp\left(\frac{\hbar \omega}{k_b [T_{loc}]_j} - 1\right)} - \frac{1}{\exp\left(\frac{\hbar \omega}{k_b T_{eq}} - 1\right)} \right) \quad (27)$$

which is either positive for all frequencies and polarizations or negative for all frequencies and polarizations. In other words, scattered particles must be replaced by particles which all have the same sign as  $e^{loc} - e_{T_{eq}}^{eq}$  and which respect the energy conservation requirement. Therefore, out of the  $\mathcal{N}_{s,j}^+ + \mathcal{N}_{s,j}^-$  selected particles, we redraw properties for  $|\mathcal{N}_{s,j}^+ - \mathcal{N}_{s,j}^-|$  of them according to the distribution (27) and delete the other selected particles. The  $|\mathcal{N}_{s,j}^+ - \mathcal{N}_{s,j}^-|$  particles to be kept are chosen randomly inside the cell  $j$  and are given the sign of  $e^{loc} - e_{T_{eq}}^{eq}$ .

This process tends to reduce the number of particles in the system and counteracts sources of particle creation within the algorithm (e.g. see boundary conditions discussed

in the next section). A bounded number of particles is essential to the method stability and the reduction process just described is a major contributor to the latter [11, 12]. Hence, in a typical problem starting from an equilibrium state that is also chosen as the control, the number of particles will first increase from zero and, at steady state, reach a constant value that can be estimated by appropriately choosing  $\mathcal{E}_{eff}^d$  as described in section 3.1. The constant value will usually be higher (but of the same order) than the estimated value: indeed, the rate of elimination of pairs of particles of opposite signs depends on the number of particles per cell and therefore on the spatial discretization chosen (the finer the discretization, the smaller the number of particles per cell and therefore the smaller the rate of elimination).

### 3.5 Boundary conditions

In phonon transport problems, various types of boundary conditions appear. Isothermal boundary conditions, similar by nature to a black body, have been used in several studies [8, 9]. Adiabatic boundaries also naturally appear [8, 20]. Recently, a class of periodic boundary conditions has also been introduced [10]. The deviational formulation adapts remarkably well to these different classes of boundary conditions.

#### 3.5.1 Adiabatic boundaries

Adiabatic boundaries reflect all incident phonons. This reflection process can be divided into two main categories: diffuse reflection and specular reflection. In both cases, it is assumed that the polarization and frequency remains the same when a phonon is reflected. The only modified parameter during the process is the traveling direction.

- i *Specular reflection* on a boundary  $\partial n$  of normal vector  $\mathbf{n}$  can be expressed, in terms of energy distribution, by

$$e(\mathbf{x}, \mathbf{k}) = e(\mathbf{x}, \mathbf{k}') \quad (28)$$

where  $\mathbf{k}' = \mathbf{k} - 2(\mathbf{k} \cdot \mathbf{n})\mathbf{n}$  and  $\mathbf{x} \in \partial n$ . Since the equilibrium distribution  $e_{T_{eq}}^{eq}$  is isotropic, then subtracting it from both sides simply yields

$$e^d(\mathbf{x}, \mathbf{k}) = e^d(\mathbf{x}, \mathbf{k}') \quad (29)$$

In other words, deviational particles are specularly reflected

- ii *Diffuse reflection* amounts to randomizing the traveling direction of a phonon incident on the boundary, in order for the population of phonons leaving the boundary to be isotropic. Since an equilibrium distribution is already isotropic, incident deviational particles are treated identically to real phonons.

### 3.5.2 Isothermal boundaries

In the case of an isothermal boundary at temperature  $T_b$ , incident phonons are absorbed, while the boundary itself, at temperature  $T_b$ , emits new phonons from the equilibrium distribution corresponding to  $T_b$ . The emitted heat flux per unit radial frequency is expressed by

$$q''_{\omega,b} = \frac{1}{4} \sum_p \frac{D(\omega, p) V_g(\omega, p) \hbar \omega}{\exp\left(\frac{\hbar \omega}{k_b T_b}\right) - 1} \quad (30)$$

Subtracting the heat flux per unit radial frequency corresponding to a boundary at equilibrium temperature, we obtain

$$q''_{\omega,b} = \frac{1}{4} \sum_p D(\omega, p) V_g(\omega, p) \hbar \omega \left( \frac{1}{\exp\left(\frac{\hbar \omega}{k_b T_b}\right) - 1} - \frac{1}{\exp\left(\frac{\hbar \omega}{k_b T_{eq}}\right) - 1} \right) \quad (31)$$

which gives the frequency distribution of emitted particles. Traveling directions must be chosen accordingly, as explained for example in [8].

### 3.5.3 Periodic unit cell boundary conditions

Heat transfer in periodic nanostructures is a subject of considerable interest in the context of many applications. Such nanostructures are considered in Hao *et al.* [10], in Huang *et al.* [21] and in Jeng *et al.* [4]. Hao *et al.* developed periodic boundary conditions that allow efficient simulation of such structures by considering only one unit cell (period). In this section we review the work of Hao *et al.* [10] and explain how the deviational particle formulation presented here lends itself naturally to this type of boundary condition. Simulations using these boundary conditions are presented in section 6.1.

We consider a 2D periodic structure depicted in Figure 3 in which square unit cells containing two rectangular voids are organised in a square lattice. Our interest focuses on determining the effective thermal conductivity of such a structure as a function of  $d$ , the degree of alignment.

The formulation introduced by Hao *et al.* amounts to stating that, at the boundaries, the deviation of the phonon distribution from the local equilibrium is periodic. Using the notations from Figure 3, this condition can be written as

$$\begin{cases} f_1^+ - f_{T_1}^{eq} = f_2^+ - f_{T_2}^{eq} \\ f_1^- - f_{T_1}^{eq} = f_2^- - f_{T_2}^{eq} \end{cases} \quad (32)$$

where  $f_{T_1}^{eq}$  and  $f_{T_2}^{eq}$  refer to the equilibrium distributions at temperatures  $T_1$  and  $T_2$ , where the superscript  $+$  denotes particles moving to the right (with respect to figure 3) and where superscript  $-$  refers to particles moving to the left. This formulation enforces at the same time the periodicity of the heat flux and a temperature gradient. In terms

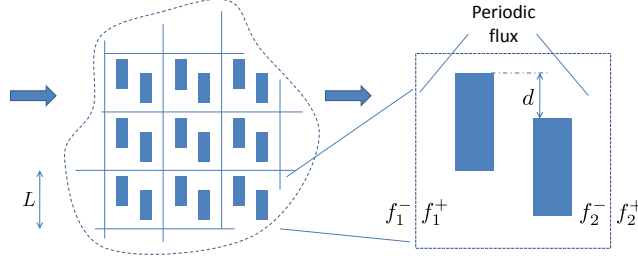


Figure 3: Example of a periodic nanostructure. Each periodic cell comprises two rectangular voids with diffusely reflecting walls. This nanostructure, and in particular the influence of the parameter  $d$ , is studied further in section 6.1

of deviational energy distributions, this relation becomes

$$\begin{cases} \hbar\omega(f_1^+ - f_{T_{eq}}^{eq} - f_{T_1}^{eq}) = \hbar\omega(f_2^+ - f_{T_{eq}}^{eq} - f_{T_2}^{eq}) \\ \hbar\omega(f_1^- - f_{T_{eq}}^{eq} - f_{T_1}^{eq}) = \hbar\omega(f_2^- - f_{T_{eq}}^{eq} - f_{T_2}^{eq}) \end{cases} \quad (33)$$

which amounts to

$$\begin{cases} e_1^{d,+} - e_{T_1}^{eq} = e_2^{d,+} - e_{T_2}^{eq} \\ e_1^{d,-} - e_{T_1}^{eq} = e_2^{d,-} - e_{T_2}^{eq} \end{cases} \quad (34)$$

Computationally, this formulation can be implemented by emitting new particles from both sides while periodically advecting the existing particles. Without any loss of generality, let us assume that  $T_1 > T_2$ . Particles emitted from the hot side originate from the distribution

$$e_1^{d,+} = e_2^{d,+} + e_{T_1}^{eq} - e_{T_2}^{eq} \quad (35)$$

Therefore, at a given point on the boundary, denoting  $\theta$  the angle with respect to the normal and  $\phi$  the azimuthal angle, the flux per unit radial frequency locally emitted from boundary 1 (“hot” side) in the solid angle  $d\Omega = \sin\theta d\theta d\phi$  can be expressed as

$$\begin{aligned} q''_{\omega,h} &= \sum_p e_1^{d,+}(\omega, \theta, \phi, p) \frac{D(\omega, p)}{4\pi} V_g(\omega, p) \cos\theta \sin\theta d\theta d\phi \\ &= \sum_p e_2^{d,+} \underbrace{\frac{D(\omega, p)}{4\pi} V_g(\omega, p) \cos\theta \sin\theta d\theta d\phi}_{\text{crossing boundary 2}} + \underbrace{(e_{T_1}^{eq} - e_{T_2}^{eq}) \frac{D(\omega, p)}{4\pi} V_g(\omega, p) \cos\theta \sin\theta d\theta d\phi}_{\text{new particles generated}} \end{aligned} \quad (36)$$

Similarly, the flux per unit radial frequency locally emitted from boundary 2 (“cold” boundary) can be expressed as

$$q''_{\omega,c} = \sum_p e_1^{d,-} \underbrace{\frac{D(\omega, p)}{4\pi} V_g(\omega, p) \cos\theta \sin\theta d\theta d\phi}_{\text{crossing boundary 1}} - \underbrace{(e_{T_1}^{eq} - e_{T_2}^{eq}) \frac{D(\omega, p)}{4\pi} V_g(\omega, p) \cos\theta \sin\theta d\theta d\phi}_{\text{new particles generated}} \quad (37)$$

Hence the boundary condition can be enforced by:

- i Moving all particles and applying periodic boundary conditions to those crossing a periodic boundary: a particle leaving the system on one side is reinserted on the other side.
- ii Generating new particles from the distribution

$$(e_{T_1}^{eq} - e_{T_2}^{eq}) \frac{D(\omega, p)}{4\pi} V_g(\omega, p) \quad (38)$$

The number of new particles is given by integrating (38) over all frequencies and polarizations and by multiplying the result by  $\pi$  to account for the integration over the solid angle  $\int_{\phi=0}^{2\pi} \int_{\theta=0}^{\pi/2} \cos \theta \sin \theta d\theta d\phi$ . The traveling direction of these particles is randomized on the half-sphere pointing into the domain and in the case of the hot boundary they are sent traveling to the right with a positive sign. Taking their mirror image, negative particles with the same properties are emitted by the cold boundary.

## 4 Validation

### 4.1 A ballistic problem

In order to validate the proposed formulation, we first consider a one-dimensional system bounded by two isothermal (3.5.2) boundaries that are sufficiently close – their distance,  $L$ , is much smaller than all phonon mean free paths – that transport can be modeled as ballistic. The system is initially at a uniform equilibrium temperature  $T_0$ , when at  $t = 0^+$  the temperature of the isothermal walls impulsively changes to  $T_0 \pm \Delta T$ .

Appendix B presents an analytical solution for the resulting transient evolution of the temperature field that is used here for comparison with our simulations. A particularly interesting case is the Debye model which, when coupled with small temperature amplitudes, allows a linearization of the general relation (55) to provide a fairly simple closed-form solution (56). Figure 4 shows a comparison between this solution and the variance-reduced Monte Carlo result. The simulation was run with  $T_{eq} = T_0$  and the phonon velocity was taken to be  $12,360 m.s^{-1}$  [10]. Excellent agreement is observed.

### 4.2 Heat flux and thermal conductivity in a thin slab

In this section we continue to validate our formulation by calculating the thermal conductivity of a thin silicon slab bounded by two diffusely reflecting walls a distance  $d$  apart in the  $z$  direction (see Figure 5). The slab is infinite in the  $x$  and  $y$  directions.

This problem is considered here because the solution can be expressed analytically. We introduce the local deviation function  $f^d = f - f^{loc}$  and, denoting the temperature gradient by  $dT/dy$ , rewrite the BTE at steady state as:

$$V_g \frac{df^{loc}}{dT} \frac{dT}{dy} \cos(\theta) + \mathbf{V}_g \nabla f^d = -\frac{f^d}{\tau} \quad (39)$$

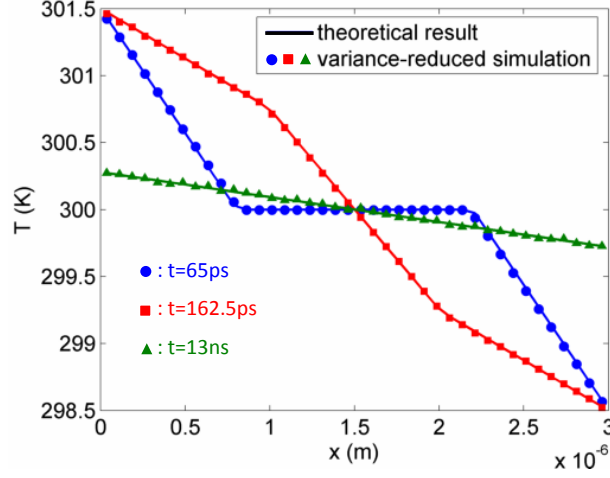


Figure 4: Transient temperature profile in a one-dimensional ballistic system whose boundary temperatures undergo an impulsive change at  $t = 0$ . Initially, the system is in equilibrium at temperature  $T_0 = 300\text{K}$ . At  $t = 0^+$ , the wall temperatures become  $T_0 \pm \Delta T$ ; here,  $\Delta T = 3\text{ K}$ .

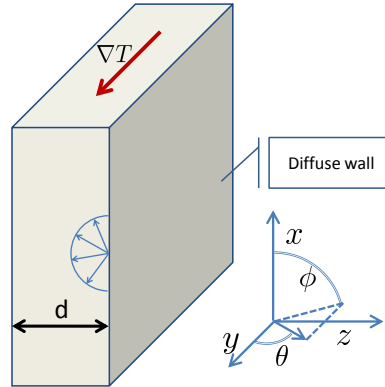


Figure 5: Heat conduction in a silicon slab due to an imposed temperature gradient in the  $y$  direction. Slab is infinite in the  $x$  and  $y$  directions.

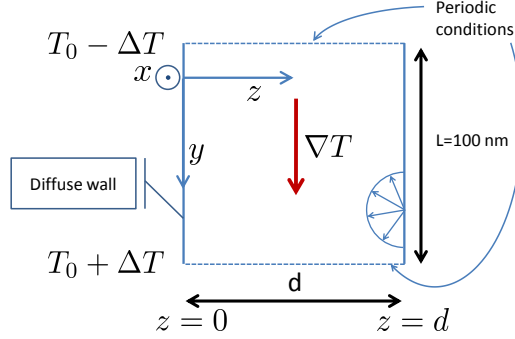


Figure 6: Simulation geometry. Boundaries at  $z = 0$  and  $z = L$  are diffusely reflecting. Infinite domain in  $y$  direction is terminated using periodic boundaries  $L = 100\text{nm}$  apart.

This equation can be solved to yield, in the coordinate system introduced in Figure 5,

$$f^d(z, \omega, p, \theta, 0 < \phi < \pi) = -\Lambda(\omega, p, T_0) \cos(\theta) \frac{df^{loc}(\omega, T_0)}{dT} \frac{dT}{dy} \left\{ 1 - \exp \left[ -\frac{z}{\Lambda(\omega, p, T_0) \sin(\theta) \sin(\phi)} \right] \right\} \quad (40)$$

$$f^d(z, \omega, p, \theta, -\pi < \phi < 0) = -\Lambda(\omega, p, T_0) \cos(\theta) \frac{df^{loc}(\omega, T_0)}{dT} \frac{dT}{dy} \left\{ 1 - \exp \left[ -\frac{z-d}{\Lambda(\omega, p, T_0) \sin(\theta) \sin(\phi)} \right] \right\} \quad (41)$$

where  $\Lambda(\omega, p, T_0)$  is the average mean free path at frequency  $\omega$ , polarization  $p$  and temperature  $T_0$ , given by

$$\Lambda(\omega, p, T_0) = V_g(\omega, p) \tau(\omega, p, T_0) \quad (42)$$

Moments of this solution can be numerically integrated to yield values for the heat flux and the thermal conductivity of the slab.

In the simulation, we calculate the thermal conductivity by measuring the steady state heat flux in response to a temperature gradient along the  $y$  axis (see Figure 6). Due to the translational symmetry of the system, we impose the temperature gradient using the periodic unit-cell formulation presented in section 3.5.3, which allows us to use a finite system size in the  $y$ -direction, taken to be  $L = 100\text{nm}$ . In order to measure the thermal conductivity at  $T_0$ , a temperature gradient is imposed by setting a target temperature of  $T_0 + \Delta T$  for the hotter of the two boundaries and  $T_0 - \Delta T$  for the colder boundary, and we proceed as explained in 3.5.3. The deviational method allows the solution of this problem for  $\Delta T \ll T_0$  (here,  $\Delta T = 0.05\text{K}$ ), in contrast to non-variance-reduced methods that would require  $\Delta T \sim T_0$  to achieve statistically significant results.



The best choice for the equilibrium (control) temperature is clearly  $T_{eq} = T_0 = 300\text{K}$ . Initializing the simulation at equilibrium at  $T_0$  is also convenient, because no particles need to be generated for the initial configuration.

Figure 7 compares the heat flux in the  $y$  direction inside a slab of silicon (see Appendix A for material parameters) of thickness  $d = 100\text{nm}$ , as computed by the deviational method, to the analytical solution. Figure 8 compares the thermal conductivity of the slab at  $T_0 = 300\text{K}$  as a function of  $d$  computed from the deviational method and from the analytical expression. Very good agreement is observed in all cases.

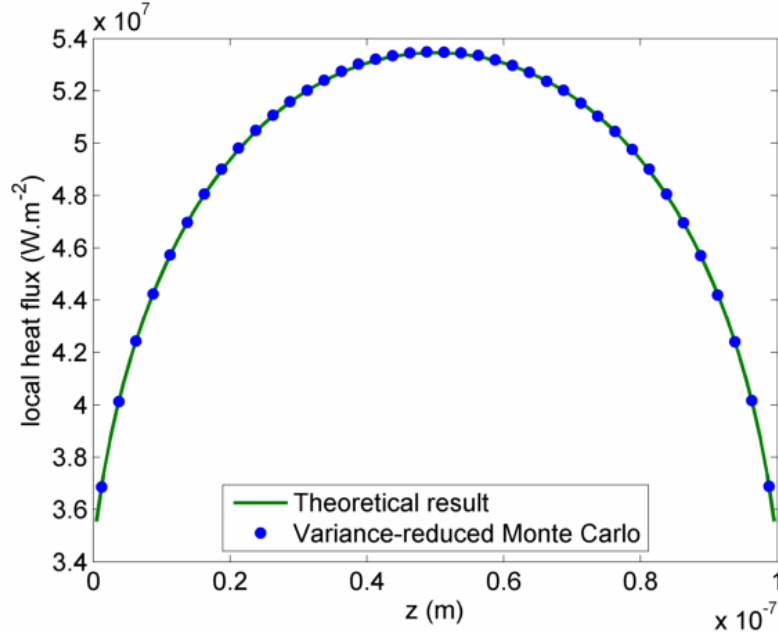


Figure 7: Spatial variation of the axial (in the  $y$  direction) heat flux in a thin film with a thickness  $d = 100\text{nm}$ , computed theoretically and compared to the result of the deviational simulation.

## 5 Computational efficiency

The variance-reduced method developed here allows substantial improvement in the relative statistical uncertainty,  $\sigma/\Delta T$ , compared to non-variance-reduced simulations. Here,  $\sigma$  is the standard deviation in the temperature measurement and  $\Delta T$  is the characteristic temperature difference (as, for example, in the validation case studied in 4.2).

Figure 9 compares the relative statistical uncertainty of the variance-reduced with the standard method. The reported data was obtained by simulating equilibrium at

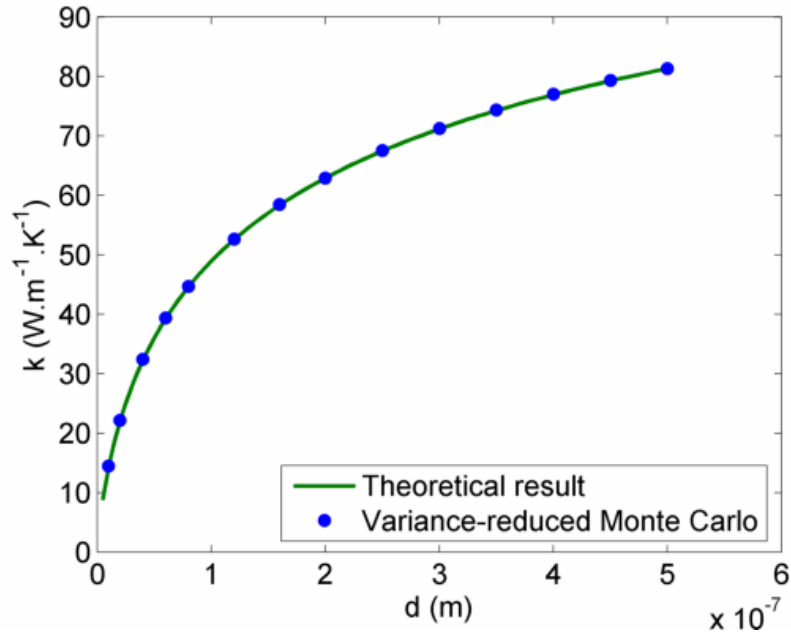


Figure 8: Theoretical values of the thin film thermal conductivity at  $T_0 = 300\text{K}$ , computed by numerical integration of the theoretical expressions (40) and (41). Comparison with the values obtained from the deviational simulation.

some temperature  $T_1$ , and defining  $\Delta T = T_1 - T_0$  as the characteristic signal that needs to be resolved. By choosing  $T_{eq} = T_0$  in the deviational method, we ensure finite deviation from equilibrium is considered and thus the statistical uncertainty is non-zero. Simulating an equilibrium state is a matter of convenience, because in non-equilibrium problems the number of particles and thus the local statistical uncertainty varies as a function of space in the deviational simulation and is thus difficult to quantify precisely; simulations of simple problems (e.g. Couette-type problems) in the past [5, 12, 13] have yielded very similar results. We also note that even though  $\sigma/\Delta T$  is strictly speaking the ratio of statistical uncertainties, it serves as a good approximation to the ratio of computational cost, because the cost of the deviational simulation is very similar to that of standard Monte Carlo methods. Specifically, the speedup provided by the deviational method is given by the **square** of the relative statistical uncertainties.

A very interesting feature of variance-reduced methods is that the standard deviation of the results is proportional to the amplitude  $\Delta T$  of the signal, as shown in Figure 9 (see also [5, 22, 23]). As a consequence, variance-reduced methods are able to provide the desired relative statistical uncertainty (signal to noise ratio) for arbitrarily low signals without requiring more computational effort. In contrast, in the case of the non-variance-reduced method, it is more computationally expensive to obtain the desired level of relative statistical uncertainty for small variations in temperature, than for large variations in temperature. In these methods, for  $\Delta T \ll T_0$ , the statistical uncertainty is approximately constant (set by equilibrium fluctuations) and thus  $\sigma/\Delta T \sim 1/\Delta T$ . As a result, the speedup offered by the variance-reduced methods scales as  $1/(\Delta T)^2$ . For example at  $\Delta T/T_0 \approx 10^{-2}$  (i.e.  $\Delta T \approx 3K$  at room temperature) the speedup is approximately 4 orders of magnitude (see Figure 9); at  $\Delta T/T_0 \approx 10^{-3}$ , the speedup is approximately 6 orders of magnitude.

## 6 Applications

In this section we present some applications of the deviational method to problems of current engineering interest. Modeling work in these areas is still ongoing; the objective of this discussion is mainly to showcase the capabilities of the proposed method.

### 6.1 Thermal conductivity of nanoporous silicon: influence of nanopore alignment

Decreasing thermal conductivity as a means of improving the thermoelectric effect has received considerable attention, and nanostructures are a novel approach towards this goal. Similarly to Huang *et al.* [21] and Jeng *et al.* [4], we assess here the thermal conductivity of novel nanostructured materials. The nanostructure considered here is made of rectangular pores as shown in Figure 3. We model it as a 2D problem (possible if the material boundaries in the directions normal to the plane shown in the figure can be approximated as specularly reflecting). Figure 10 shows the periodic cell considered and defines the parameter  $d$  that we use to describe the spatial distribution of the

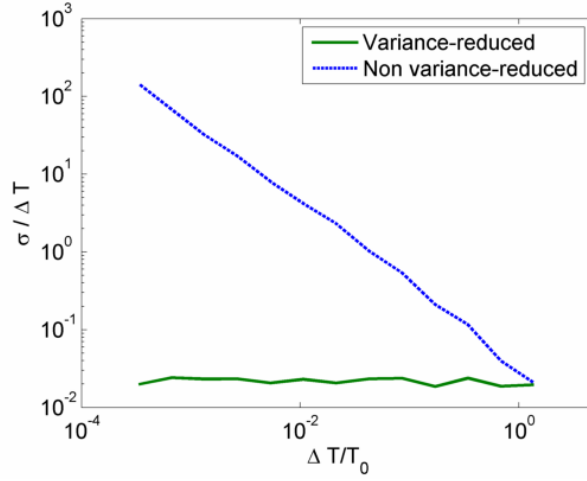


Figure 9: Comparison of relative statistical uncertainties for equilibrium systems at temperature  $T_1$  with  $\Delta T = T_1 - T_0$  and  $T_0 = 300K$ .

pores. The thermal conductivity in the  $y$  direction is measured by imposing periodic unit-cell boundary conditions as explained in section 3.5.3 with a temperature difference of 0.1K across the unit cell. Using the data of Appendix A, the contributions of the different mean free paths to the bulk thermal conductivity can be calculated. A plot of the effective thermal conductivity, as computed with the deviational variance-reduced method, is displayed in Figure 10. The thermal conductivity is reduced by almost a factor of 2 because of this geometrical effect. This highlights the importance of ballistic effects.

The importance of ballistic effects is further highlighted by Figure 11 which shows that at  $T_0 = 300K$ , mean free paths from 50nm to  $10\mu m$  contribute significantly to the thermal conductivity of the bulk material; the presence of voids with period of 100nm affects the contribution of all mean free paths, but completely suppresses the contribution of all mean free paths greater than about one micrometer. Tuning the alignment parameter, decreases further the contribution of the mean free paths between 50nm and  $1\mu m$ .

## 6.2 Simulation of thermal conductivity spectroscopy

Figure 12 depicts an experimental setup developed in the MIT Nanoengineering Lab [25] as a prototype “thermal conductivity spectroscopy” system. This experiment is based on pump-probe transient thermorefectance, in which a pump pulse is used to change the physical properties of a sample and a probe pulse is used to measure the change. In this experiment, a thin film of aluminum (thickness between 50 and 100nm) is deposited on a silicon wafer and is initially at uniform temperature, say 300K. At

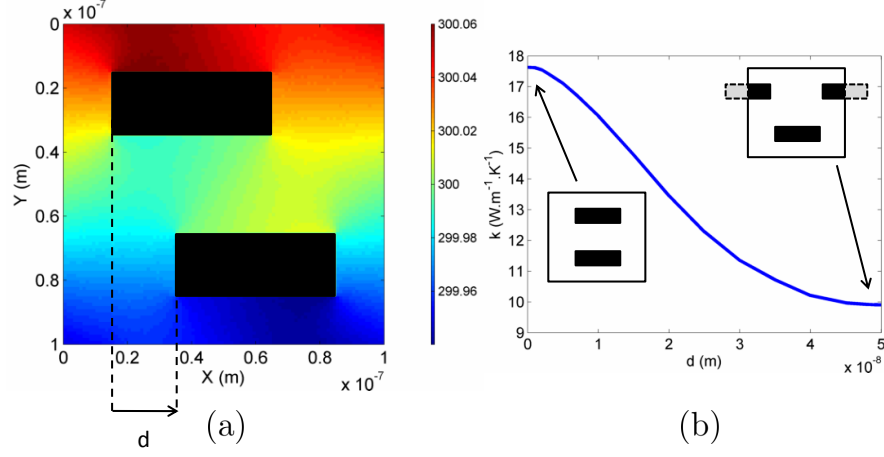


Figure 10: (a) Temperature field in a unit cell of a periodic nanoporous material. (b) Thermal conductivity as a function of parameter  $d$ .

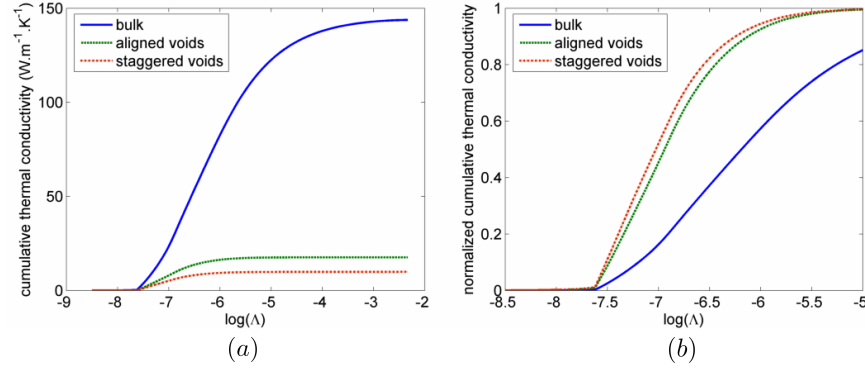


Figure 11: (a) Thermal conductivity accumulation as a function of the mean free path. The bulk conductivity was computed by numerical integration of the thermal conductivity per unit frequency  $\tau v^2 C_\omega / 3$  [15, 24, 1]; here,  $C_\omega$  is the heat capacity per frequency unit. (b) Normalized thermal conductivity accumulation, highlighting the influence of ballistic effects on the thermal conductivity.

$t = 0$ , localized laser irradiation creates a hot spot, shown in figure 12 as centered on the origin ( $r = 0, z = 0$ ) of the coordinate system. A reliable description of the subsequent evolution of the temperature field is central to interpreting the experimental results and creating a means for inferring phonon mean free paths (the goal of this experiment) from experimental measurements (e.g. surface temperature)

Given the scale of the aluminum slab, the impulsive nature of the heating, and the short duration of the phenomenon, phonon ballistic behavior needs to be accounted for, necessitating a Boltzmann treatment. However, this problem is very difficult (if not impossible) to simulate using standard Monte Carlo methods: the initial perturbation to the temperature field is small in amplitude (see below) which makes resolution of transient results very costly. Moreover, the need to simulate early as well as late times and avoid artifacts from artificial domain termination makes the simulation of a large computational domain necessary, even though the original hot spot is very small. In traditional Monte Carlo methods, this large computational domain would need to be filled with particles.

The method proposed makes this calculation possible. Simulating the deviation from equilibrium allows the calculation to proceed using zero particles in regions not yet affected by the heating pulse. Thus, in addition to variance reduction which removes the limitations associated with statistical uncertainty, simulating the deviation from equilibrium simultaneously considerably reduces the computational cost resulting from the multiscale nature of this problem. We also note that by taking the equilibrium distribution at 300K, the simulation only has positive particles. Hence there will be no cancellation of particles and the entire simulation will run with a fixed amount of particles.

In practice, one can exploit the cylindrical symmetry in order to reduce the problem dimensionality: the resulting temperature field is expected to depend only on the depth  $z$  and on the distance from the center of the pulse,  $r$ . Therefore, we can use toroidal cells to sample the temperature and process the scattering. The only drawback is that cells near the center, at small radius, will have a smaller volume and will sample the temperature over a smaller number of particles, thus yielding noisier results in these regions.

### 6.2.1 Initial condition

As stated above, since the material is originally at equilibrium at  $T_0 = 300\text{K}$  it is most convenient, but also computationally efficient, to choose  $T_{eq} = T_0$ . Laser irradiation introduces a heating effect in a thin layer close to the irradiated surface which has been parametrized [15] using the following expression

$$\Delta T(r, z) = T - T_0 = A \exp\left(-\frac{2r^2}{R_0^2} - \beta z\right) \quad (43)$$

with  $A = 1\text{K}$ ,  $R_0 = 15\mu\text{m}$  and  $\beta^{-1} = 7\text{nm}$ . This expression is used here as an initial condition for the material temperature. Regions for which  $\Delta T < .005K$  were taken to

be at equilibrium at  $T_0 = T_{eq}$  (no particles).

### 6.2.2 Interface modeling

The top surface of the aluminum material ( $z = 0$ ) is modeled as a diffusely reflecting wall.

Modeling the interface between the two materials accurately is still an active area of research. Here, we chose to use a recently developed model [15, 26] which relates the transmissivity to the interface conductance  $G$  through the expression

$$\langle P_{1 \rightarrow 2} C_1 V_{g,1} \rangle = \frac{2}{\frac{1}{\langle C_1 V_{g,1} \rangle} + \frac{1}{\langle C_2 V_{g,2} \rangle} + \frac{1}{2G}} \quad (44)$$

Here,  $P_{i \rightarrow j}$  denotes the probability for a phonon to pass through the interface from material  $i$  to  $j$ ; the brackets denote integration over frequency and sum over polarization, while  $C_1$  and  $C_2$  denote the volume heat capacity per unit frequency in media 1 and 2, respectively. In this model, we assume that the interface is totally diffuse: the direction of an incident particle is reset regardless of the transmission or reflection of the particle, while its frequency and polarization are retained [27]. For the interface conductance  $G$ , we use the experimental value  $G = 1.1 \times 10^8 \text{ W m}^{-2} \text{ K}^{-1}$  [26].

We also utilize the expression [27]

$$D_1(\omega, p) V_{1,g}(\omega, p) f_{T_0}^{eq} P_{1 \rightarrow 2}(\omega, p) = D_2(\omega, p) V_{2,g}(\omega, p) f_{T_0}^{eq} P_{2 \rightarrow 1}(\omega, p) \quad (45)$$

which relates the probability for a phonon with radial frequency  $\omega$  and polarization  $p$  to pass through the interface from 1 to 2 to the probability to pass from 2 to 1.

We can easily verify that relation (45) applies when the deviational energy  $e^d$  is used instead of the phonon distribution. Additionally, expression (44) which relies, among other things, on (45) [15, 26], also remains unchanged when applied to deviational particles.

Following [15, 26], we let  $P_{1 \rightarrow 2}$  be a constant (which makes it easy to calculate from (44)) and deduce  $P_{2 \rightarrow 1}$  from (45). In our case we chose to set  $P_{Al \rightarrow Si}$  constant, except for the high frequency transverse acoustic modes; since the cutoff frequency of the TA branch in Si is lower than the TA cutoff frequency in Al, phonons with such frequencies must undergo total reflection [15]. Similarly, LA phonons in Si whose frequency is above the aluminum LA branch cutoff frequency are totally reflected.

### 6.2.3 Domain termination

At long times, phonons may travel far from the hot spot. In order to avoid discretizing an infinite domain with computational cells (for calculating the temperature) we restrict our discretization to a finite (but large) “nominal” domain. In order to simulate accurately and consistently the actual system, we keep track of the particles even after they have left the nominal part of the domain.

Particles that leave this domain are not sampled (for calculating the temperature and pseudo temperature), but are still scattered by assuming a local temperature of 300K as an input parameter for the relaxation time. This amounts to a linearization of the collision operator at  $T = 300\text{K}$  and is based on the reasonable assumption that sufficiently far from the heating source, the temperature is very close to 300K. Particles that leave the nominal part of the domain may reenter the nominal domain, hence ensuring a rigorous treatment of the semi-infinite region.

Particular care is taken to ensure that the frequency and polarization of a particle is drawn from the correct distribution, because energy conservation—built into the simulation method—requires that the number of particles is conserved by the scattering process and is inconsistent with approximations which do not conserve energy. For example, setting  $T_{loc} = 300\text{K}$  is inconsistent with energy conservation because  $e^{loc}(T_{loc} = 300\text{K}) - e^{eq} = 0$ , which implies no particle generation, which in the presence of particle deletion due to the term  $-e^d/\tau$  leads to net particle and thus energy loss. This situation can be rectified by allowing the temperature at the particle position to be different from  $T_{eq}$ ; specifically, we write  $T = T_{eq} + \epsilon$  and expand

$$\frac{D(\omega, p)(e^{loc} - e_{T_{eq}}^{eq})}{\tau(\omega, p, T_{eq})} \approx \frac{D(\omega, p)}{\tau(\omega, p, T_{eq})} \frac{\partial e_{T_{eq}}^{eq}}{\partial T} \epsilon \quad (46)$$

Frequencies and polarizations are thus drawn from

$$\frac{D(\omega, p)}{\tau(\omega, p, T_{eq})} \frac{\partial e_{T_{eq}}^{eq}}{\partial T} \quad (47)$$

since (46) once normalized, does not depend on the local  $\epsilon$ . As before, energy conservation is ensured by simply conserving the particles.

In addition to providing a method for terminating simulations, this approach represents a promising avenue for treating the entire simulation domain in the limit that linearization of the collision operator is appropriate. The advantage of this formulation is significant reduction in computational cost because evaluation of the local temperature and pseudo-temperature is not required every timestep. Further details will be presented in a future publication.

#### 6.2.4 Simulation results

Figure 13 and 14 show that the variance-reduced method developed here can calculate the temperature field with small statistical uncertainty. This is remarkable given the minute temperature differences ( $O(0.01)\text{K}$ ) present in this problem, especially at late times. For such temperatures, according to Figure 9, the speedup compared to a standard Monte Carlo method is on the order of  $10^9$ .

Figure 14 compares our simulation results with a numerical solution of the heat conduction equation (Fourier’s Law). The differences between the two predictions are a result of non-diffusive (ballistic/transitional) effects. The detailed information available



in simulations of this phenomenon can assist in the development of methodologies for characterizing carrier mean free paths from comparisons such as the one shown in Figure 14. Here, we note that the present calculation does not account for thermal transport by electrons in aluminum. This was neglected in the interest of simplicity and because the primary focus of this experiment is transport through the silicon substrate [15]. Thermal transport by electrons in aluminum will be considered and evaluated in a future publication.

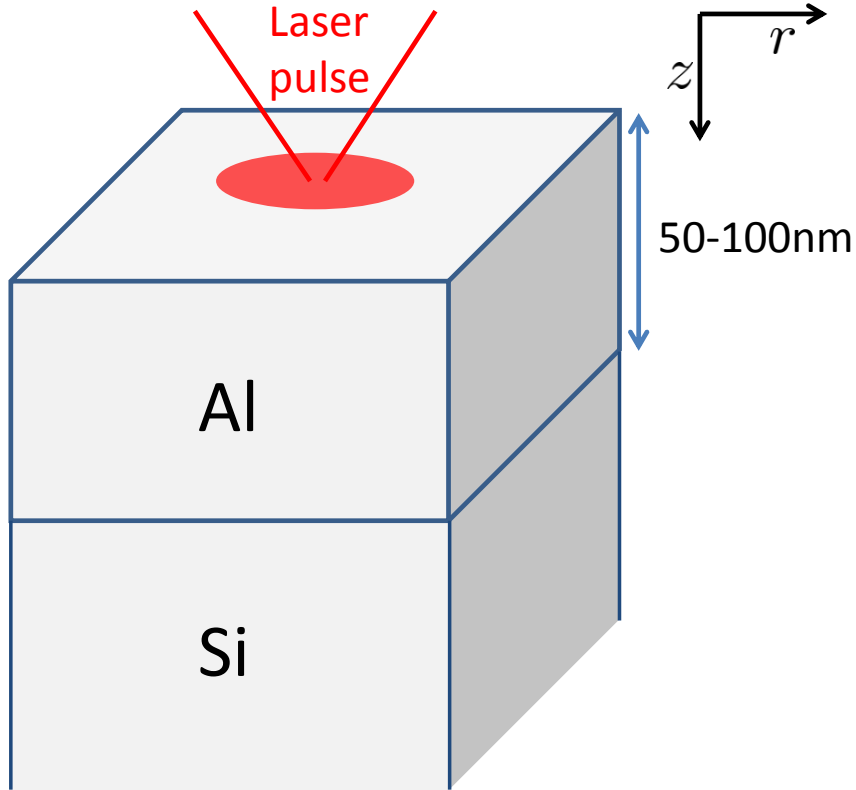


Figure 12: System composed of a slab of aluminum on a semi-infinite silicon wafer, used for transient thermoreflectance (TTR) experiments. At  $t=0$ , a laser pulse induces a temperature field  $T(r, z, t)$ . The temperature field evolution after the pulse is computed by assuming that the aluminum surface is adiabatic.

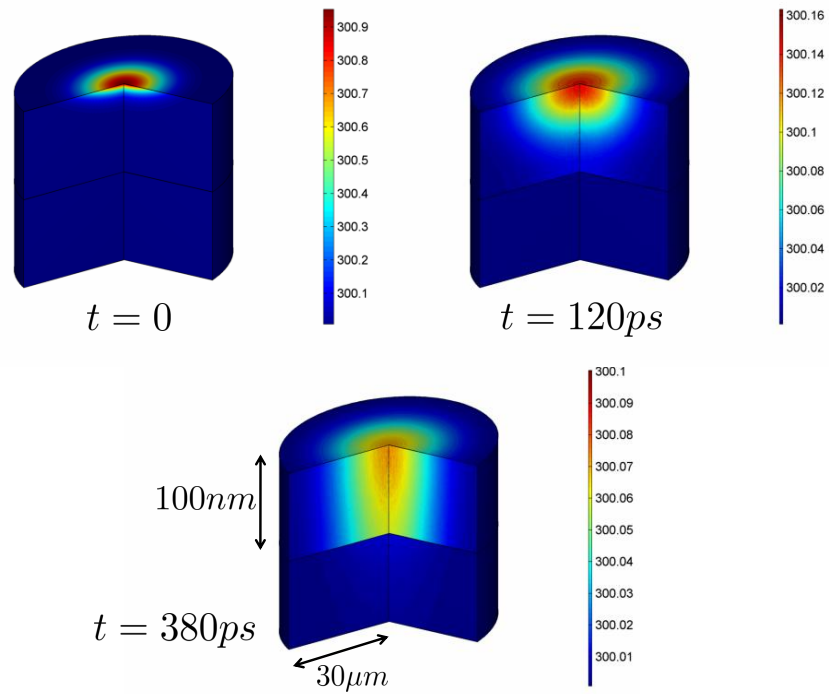


Figure 13: Variance-reduced temperature field in aluminum slab and the silicon wafer after initial heating by a laser pulse. The picture shows the aluminum slab (100nm thickness) and a portion of the silicon wafer (100nm thickness).

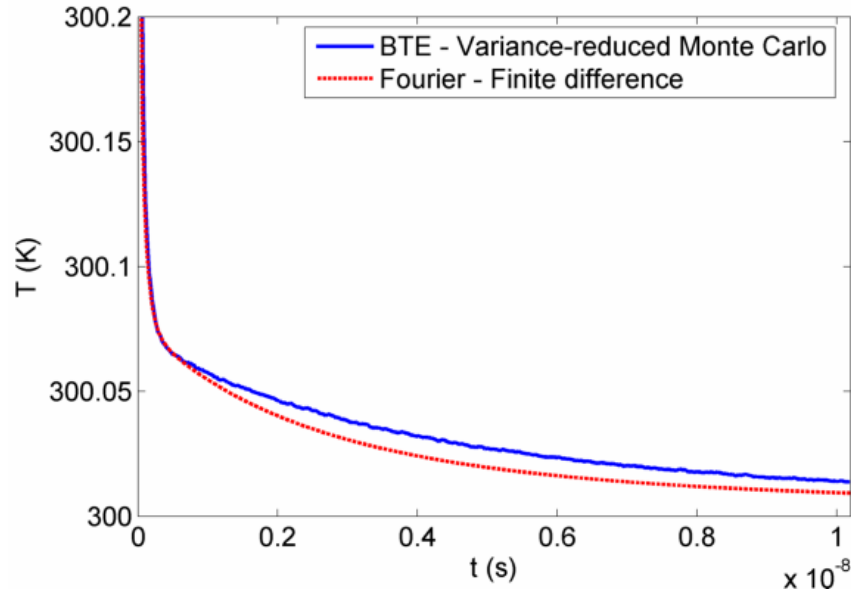


Figure 14: Surface temperature at the hot spot (averaged over the region  $0 \leq r \leq 2\mu m$ ,  $0 \leq z \leq 5nm$ ) as a function of time after initial heating by laser pulse. The difference with the solution based on the Fourier model is a result of ballistic effects.

## 7 Discussion

We have shown that efficient and accurate algorithms for solving the BTE with significantly reduced statistical uncertainty can be developed by focusing on the deviation from a nearby equilibrium within an energy-based formulation. The energy-based formulation facilitates exact energy conservation thus improving the simulation fidelity, while the variance reduction is made possible by the deterministic information inherent in the Bose-Einstein distribution which describes the nearby equilibrium. The proposed method was validated using analytical solutions of the Boltzmann Transport Equation. Very good agreement with the analytical results was found.

The proposed algorithm was used to study the effect of porosity on the effective thermal conductivity of pure silicon. Our results show that staggering periodically arranged voids at small scales exploits ballistic shading to effect reduction in the effective thermal conductivity. A more systematic investigation of the effects of porosity on the effective conductivity of silicon—including anisotropic effects—will be the subject of future work.

We also presented simulations of a recently developed experimental technique known as thermal conductivity spectroscopy, in which the transient response of a thin aluminum slab over a silicon wafer to a localized heating induced by a laser pulse is used to infer properties of heat carriers. This simulation required the development of a domain termination algorithm for rigorously treating deviational particles as they travel to regions far from the heating source, without having to sample these particles everywhere in this semi-infinite region. The algorithm developed corresponds to a linearization of the collision operator and may, in fact, form the basis of a significantly more efficient simulation approach valid in cases where linearization is appropriate.

In addition to illustrating the benefits of variance reduction, simulations of the thermal conductivity spectroscopy problem also showcase the value of the proposed simulation approach as a new multiscale method: in contrast to typical multiscale methods which focus on spatially decomposing the domain into the particle and continuum subdomains, the present algorithm achieves a seamless transition from one description to the other by instead *algebraically* decomposing the distribution function into a part described by particles and a part described deterministically [28]. Although here the simplest such implementation has been presented (deterministic description is equilibrium at temperature  $T_0 \neq T_0(\mathbf{x}, t)$ ), deviational algorithms featuring a deterministic description that varies as a function of space ( $e^{eq} = e^{eq}(\mathbf{x})$ ) have been developed [12, 13] and shown to achieve improved variance reduction as  $Kn \rightarrow 0$  [13], albeit at the cost of a moderately more complex algorithm. In the problem considered here, the continuum behavior at large distances from the heat source is in fact equilibrium at  $T_0$  and thus the present algorithm is sufficient. However, in other problems where a local equilibrium is present in large parts of the domain, algebraic decomposition using  $e^{eq} = e^{eq}(\mathbf{x})$  will be able to provide considerable computational savings by considerably reducing the number of particles required for its simulation.

## 8 Acknowledgements

The authors are indebted to Colin Landon, Gregg Radtke and Austin Minnich for many useful comments and discussions. This work was supported in part by the Singapore-MIT Alliance. J-P. M. Péraud gratefully acknowledges financial support from Ecole Nationale des Ponts et Chaussées and the MIT Department of Materials Science and Engineering through a Graduate Fellowship.

## A Numerical data for scattering rates

In the simulations presented here we use data for the dispersion relations and for the relaxation times of phonons in Al and Si. Dispersion relations are adapted from the experimentally measured dispersion in the [100] direction ([29] for Al, [30, 15] for Si).

For Al, as in [26, 15], we assume a constant relaxation time chosen to match the desired lattice thermal conductivity. We therefore take the value

$$\tau_{Al} = 10^{-11} \text{s} \quad (48)$$

For Si, we use the expressions from [31], with constants from [15]. Relaxation times for acoustic modes are given by

phonon-phonon scattering, LA	$\tau_L^{-1} = A_L \omega^2 T^{1.49} \exp\left(\frac{-\theta}{T}\right)$
phonon-phonon scattering, TA	$\tau_T^{-1} = A_T \omega^2 T^{1.65} \exp\left(\frac{-\theta}{T}\right)$
impurity scattering	$\tau_I^{-1} = A_I \omega^4$
boundary scattering	$\tau_B^{-1} = w_b$

where the constants take the following values

Parameter	$A_L$	$A_T$	$\theta$	$A_I$	$w_b$
Value (in SI units)	$2 \times 10^{-19}$	$1.2 \times 10^{-19}$	80	$3 \times 10^{-45}$	$1.2 \times 10^6$

The total relaxation time for a given polarization is obtained using the Matthiessen rule

$$\tau^{-1} = \sum_i \tau_i^{-1} \quad (49)$$

Optical phonons in Si are considered immobile (Einstein model). Einstein's model states that the contribution of optical phonons to the vibrational energy per unit volume in a crystal is given by [1]

$$U = \frac{N_p N' \hbar \omega_E}{V [\exp(\hbar \omega_E / k_b T) - 1]} \quad (50)$$

where  $N_p = 3$  is the number of polarizations,  $N' = 1$  is the number of optical states per lattice point,  $\omega_E$  is the Einstein radial frequency ( $\omega_E = 9.1 \times 10^{13} \text{s}^{-1}$  [30, 15]),  $V$  is the volume of a lattice point (with a lattice constant  $a = 5.43 \text{\AA}$ ,  $V = a^3/4 = 4 \times 10^{-29} \text{m}^3$ ).

For the relaxation time of optical phonons, we use the value [32]

$$\tau_O = 3 \times 10^{-12} \text{s} \quad (51)$$

## B Derivation of the transient ballistic 1D solution

Following the impulsive change of temperature at the walls from  $T_0$  to  $T_l = T_0 + \Delta T$  and  $T_r = T_0 - \Delta T$ , thermalized phonons at temperature  $T_r$  and  $T_l$  are emitted from the “right” and “left” wall, respectively (see Figure 15).

For some arbitrary location  $x$ , for a given frequency, polarization and time, the angular space can be divided into 3 distinct domains characterized by two angles  $\theta_r(x, \omega, p, t)$  and  $\theta_l(x, \omega, p, t)$  as depicted in Figure 15. Phonons described by  $0 < \theta < \theta_l$  were emitted by the left wall at a time  $t > 0$ . Phonons described by  $\theta_l < \theta < \pi - \theta_r$  have been present in the system since  $t=0$ . Phonons described by  $\pi - \theta_r < \theta < \pi$  were emitted by the right wall at a time  $t > 0$ .

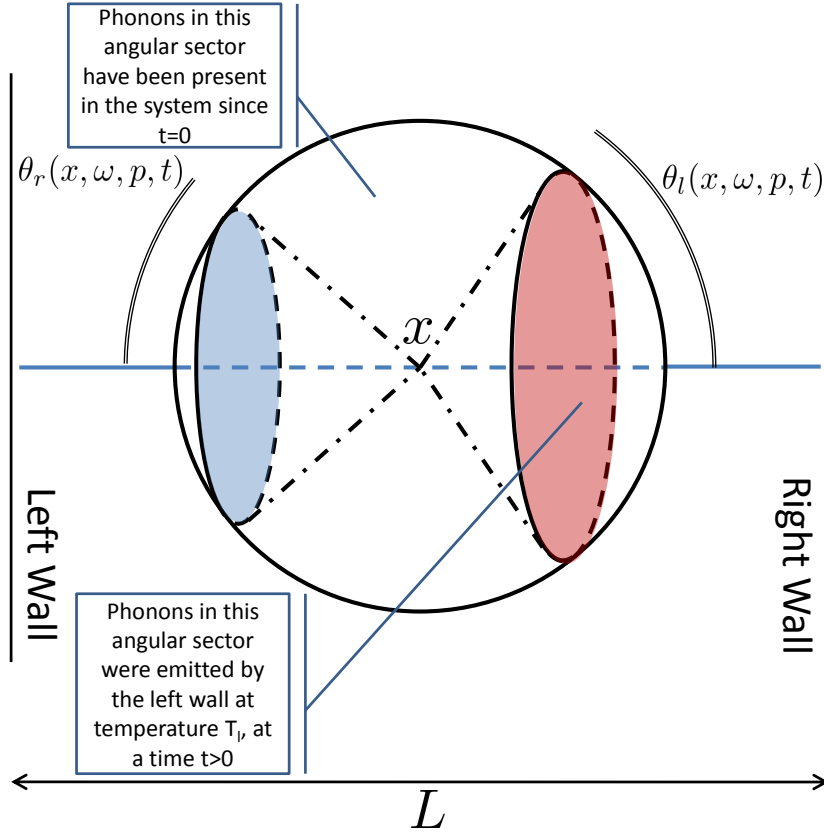


Figure 15: At a given point in space, the solid angle can be divided into three distinct regions in which the distribution of phonons is known; here,  $\theta_l$  is given by  $\cos(\theta_l) = x/(V_g(\omega, p)t)$ , while  $\theta_r$  is given by  $\cos(\theta_r) = (L - x)/(V_g(\omega, p)t)$

The energy can therefore be written as

$$E_V(x, t) = \frac{1}{2} \sum_p \left\{ \int_{\omega} \int_{\theta=0}^{\theta_l(x, \omega, p, t)} e_{T_l}^{eq}(\omega) D(\omega, p) \sin(\theta) d\theta d\omega \dots \right. \\ \left. + \int_{\omega} \int_{\theta=\theta_l(x, \omega, p, t)}^{\pi-\theta_r(x, \omega, p, t)} e_{T_0}^{eq}(\omega) D(\omega, p) \sin(\theta) d\theta d\omega \dots \right. \\ \left. + \int_{\omega} \int_{\theta=\pi-\theta_r(x, \omega, p, t)}^{\pi} e_{T_r}^{eq}(\omega) D(\omega, p) \sin(\theta) d\theta d\omega \right\} \quad (52)$$

From geometrical considerations

$$\cos(\theta_r(x, \omega, p, t)) = \min\left(1, \frac{L-x}{V_g(\omega, p)t}\right) = 1 - \left(1 - \frac{L-x}{V_g(\omega, p)t}\right) H\left(1 - \frac{L-x}{V_g(\omega, p)t}\right) \quad (53)$$

$$\cos(\theta_l(x, \omega, p, t)) = \min\left(1, \frac{x}{V_g(\omega, p)t}\right) = 1 - \left(1 - \frac{x}{V_g(\omega, p)t}\right) H\left(1 - \frac{x}{V_g(\omega, p)t}\right) \quad (54)$$

where  $H$  is the Heaviside function. Proceeding to the integration in  $\theta$ , the energy density is given by

$$E_V(x, t) = \frac{1}{2} \sum_p \left\{ \int_{\omega} \left(1 - \frac{x}{V_g(\omega, p)t}\right) H\left(1 - \frac{x}{V_g(\omega, p)t}\right) e_{T_l}^{eq}(\omega) D(\omega, p) d\omega \right. \\ + \int_{\omega} \left(1 - \frac{L-x}{V_g(\omega, p)t}\right) H\left(1 - \frac{L-x}{V_g(\omega, p)t}\right) e_{T_r}^{eq}(\omega) D(\omega, p) d\omega \\ + \int_{\omega} \left[1 - \left(1 - \frac{x}{V_g(\omega, p)t}\right) H\left(1 - \frac{x}{V_g(\omega, p)t}\right)\right] e_{T_0}^{eq}(\omega) D(\omega, p) d\omega \\ \left. + \int_{\omega} \left[1 - \left(1 - \frac{L-x}{V_g(\omega, p)t}\right) H\left(1 - \frac{L-x}{V_g(\omega, p)t}\right)\right] e_{T_0}^{eq}(\omega) D(\omega, p) d\omega \right\} \quad (55)$$

The temperature  $T = T(x, t)$  is obtained by numerically finding the Bose-Einstein distribution corresponding to this energy density.

Using the Debye model and considering small temperature changes ( $|T_r - T_0| \ll T_0$  and  $|T_l - T_0| \ll T_0$ ), the resulting temperature field can be expressed in a simpler form. The first assumption allows the removal of the frequency and polarization dependence on the group velocity, while the second assumption allows the linearization of the Bose-Einstein terms in the integrals. Several simplifications can then be carried out to yield the following expression for the temperature field

$$\Delta T(x, t) = \frac{1}{2} \left(1 - \frac{x}{V_g t}\right) H\left(1 - \frac{x}{V_g t}\right) \Delta T_l + \frac{1}{2} \left(1 - \frac{L-x}{V_g t}\right) H\left(1 - \frac{L-x}{V_g t}\right) \Delta T_r \quad (56)$$



## References

- [1] G. Chen, *Nanoscale energy transport and conversion*. 2005.
- [2] A. Majumdar, “Microscale heat-conduction in dielectric thin-films,” *Journal of Heat Transfer-Transactions of the ASME*, vol. 115, pp. 7–16, FEB 1993.
- [3] G. Chen, M. S. Dresselhaus, G. Dresselhaus, J.-P. Fleurial, and T. Caillat, “Recent developments in thermoelectric materials,” *International Materials Reviews*, vol. 48, pp. 45–66, FEB 2003.
- [4] M.-S. Jeng, R. Yang, D. Song, and G. Chen, “Modeling the thermal conductivity and phonon transport in nanoparticle composites using Monte Carlo simulation,” *Journal of Heat Transfer-Transactions of the ASME*, vol. 130, p. 042410, APR 2008.
- [5] L. L. Baker and N. G. Hadjiconstantinou, “Variance reduction for Monte Carlo solutions of the Boltzmann equation,” *Physics of Fluids*, vol. 17, no. 051703, pp. 1–4, 2005.
- [6] G. A. Bird, *Molecular Gas Dynamics and the Direct Simulation of Gas Flows*,. Clarendon Press, Oxford, 1994.
- [7] R. B. Peterson, “Direct simulation of phonon-mediated heat-transfer in a Debye crystal,” *Journal of Heat Transfer-Transactions of the ASME*, vol. 116, pp. 815–822, NOV 1994.
- [8] S. Mazumder and A. Majumdar, “Monte Carlo study of phonon transport in solid thin films including dispersion and polarization,” *Journal of Heat Transfer-Transactions of the ASME*, vol. 123, pp. 749–759, AUG 2001.
- [9] D. Lacroix, K. Joulain, and D. Lemonnier, “Monte Carlo transient phonon transport in silicon and germanium at nanoscales,” *Physical Review B*, vol. 72, p. 064305, AUG 2005.
- [10] Q. Hao, G. Chen, and M.-S. Jeng, “Frequency-dependent Monte Carlo simulations of phonon transport in two-dimensional porous silicon with aligned pores,” *Journal of Applied Physics*, vol. 106, p. 114321, DEC 1 2009.
- [11] T. M. M. Homolle and N. G. Hadjiconstantinou, “Low-variance deviational simulation Monte Carlo,” *Physics of Fluids*, vol. 19, p. 041701, APR 2007.
- [12] T. M. M. Homolle and N. G. Hadjiconstantinou, “A low-variance deviational simulation Monte Carlo for the Boltzmann equation,” *Journal of Computational Physics*, vol. 226, pp. 2341–2358, OCT 1 2007.

- [13] G. A. Radtke and N. G. Hadjiconstantinou, “Variance-reduced particle simulation of the Boltzmann transport equation in the relaxation-time approximation,” *Physical Review E*, vol. 79, p. 056711, MAY 2009.
- [14] G. A. Radtke, N. G. Hadjiconstantinou, and W. Wagner, “Low-noise Monte Carlo simulation of the variable hard sphere gas,” *Physics of fluids*, vol. 23, p. 030606, MAR 2011.
- [15] A. J. Minnich, *Exploring Electron and Phonon Transport at the Nanoscale for Thermoelectric Energy Conversion*. PhD thesis, Massachusetts Institute of Technology, 2011.
- [16] Y. K. Koh and D. G. Cahill, “Frequency dependence of the thermal conductivity of semiconductor alloys,” *Physical Review B*, vol. 76, no. 075207, 2007.
- [17] P. G. Klemens, “Thermal conductivity and lattice vibration modes,” *Solid State Physics*, vol. 7, pp. 1–98, 1958.
- [18] A. Mittal and S. Mazumder, “Monte Carlo study of phonon heat conduction in silicon thin films including contributions of optical phonons,” *Journal of Heat Transfer-Transactions of the ASME*, vol. 132, p. 052402, MAY 2010.
- [19] G. A. Radtke, *Efficient Simulation of Molecular Gas Transport for Micro- and Nanoscale Applications*. PhD thesis, Massachusetts Institute of Technology, 2011.
- [20] D. Lacroix, K. Joulain, D. Terris, and D. Lemonnier, “Monte Carlo simulation of phonon confinement in silicon nanostructures: Application to the determination of the thermal conductivity of silicon nanowires,” *Applied Physics Letters*, vol. 89, p. 103104, SEP 4 2006.
- [21] M.-J. Huang, T.-C. Tsai, L.-C. Liu, M.-S. Jeng, and C.-C. Yang, “A fast Monte-Carlo solver for phonon transport in nanostructured semiconductors,” *Cmes-Computer Modeling in Engineering And Sciences*, vol. 42, pp. 107–129, MAR 2009.
- [22] N. G. Hadjiconstantinou, “The limits of Navier-Stokes theory and kinetic extensions for describing small-scale gaseous hydrodynamics,” *Physics of Fluids*, vol. 18, p. 111301, NOV 2006.
- [23] N. G. Hadjiconstantinou, G. A. Radtke, and L. L. Baker, “On variance-reduced simulations of the Boltzmann transport equation for small-scale heat transfer applications,” *Journal of Heat Transfer-Transactions of the ASME*, vol. 132, p. 112401, NOV 2010.
- [24] J.-P. M. Péraud, “Low variance methods for Monte Carlo simulation of phonon transport,” Master’s thesis, Massachusetts Institute of Technology, 2011.

- [25] A. J. Minnich, G. Chen, S. Mansoor, and B. S. Yilbas, “Spectral phonon transport properties of silicon based on molecular dynamics simulations and lattice dynamics,” *Journal of Computational and Theoretical Nanoscience*, vol. 5, no. 2, pp. 141–152, 2011.
- [26] A. J. Minnich, G. Chen, S. Mansoor, and B. S. Yilbas, “Quasi-ballistic heat transfer studied using the frequency-dependent Boltzmann transport equation,” *In preparation*, 2011.
- [27] G. Chen, “Thermal conductivity and ballistic-phonon transport in the cross-plane direction of superlattices,” *Physical Review B*, vol. 57, pp. 14958–14973, JUN 15 1998.
- [28] G. A. Radtke, J.-P. M. Péraud, and N. G. Hadjiconstantinou, “On efficient simulations of multiscale kinetic transport,” *Philosophical Transactions of the Royal Society A (Submitted)*.
- [29] R. Stedman and G. Nilsson, “Dispersion relations for phonons in Aluminum at 80 and 300K,” *Physical Review*, vol. 145, pp. 492–500, MAY 1966.
- [30] <http://www.ioffe.ru/SVA/NSM/Semicond/Si/mechanic.html>.
- [31] A. S. Henry and G. Chen, “Spectral phonon transport properties of silicon based on molecular dynamics simulations and lattice dynamics,” *Journal of Computational and Theoretical Nanoscience*, vol. 5, pp. 141–152, FEB 2008.
- [32] P. G. Klemens, “Anharmonic decay of optical phonons,” *Physical Review*, vol. 148, pp. 845–848, Aug 1966.